NeuroImage: Clinical 38 (2023) 103373

Contents lists available at ScienceDirect

NeuroImage: Clinical

journal homepage: www.elsevier.com/locate/ynicl

Neuroinflammation and amyloid deposition in the progression of mixed Alzheimer and vascular dementia

Chunwei Ying [a,c,1], Peter Kang [b,1], Michael M. Binkley [b], Andria L. Ford [b,c], Yasheng Chen [b], Jason Hassenstab [b,d], Qing Wang [c,d], Jeremy Strain [b], John C. Morris [d], Jin-Moo Lee [a,b,c], Tammie L.S. Benzinger [c,d,e], Hongyu An [a,b,c,*]

[a] Department of Biomedical Engineering, Washington University in St. Louis, USA
[b] Department of Neurology, Washington University School of Medicine, USA
[c] Mallinckrodt Institute of Radiology, Washington University School of Medicine, USA
[d] Knight Alzheimer Disease Research Center, Washington University School of Medicine, USA
[e] Department of Neurosurgery, Washington University School of Medicine, USA

ARTICLE INFO

Keywords:
Neuroinflammation
Amyloid beta peptides
White matter hyperintensities
Vascular contributions to cognitive impairment and dementia
Alzheimer's disease

ABSTRACT

Background: Alzheimer's disease (AD) and vascular contributions to cognitive impairment and dementia (VCID) pathologies coexist in patients with cognitive impairment. Abnormal amyloid beta (Aβ) deposition is the hallmark pathologic biomarker for AD. Neuroinflammation may be a pathophysiological mechanism in both AD and VCID. In this study, we aimed to understand the role of neuroinflammation and Aβ deposition in white matter hyperintensities (WMH) progression and cognitive decline over a decade in patients with mixed AD and VCID pathologies.
Methods: Twenty-four elderly participants (median [interquartile range] age 78 [64.8, 83] years old, 14 female) were recruited from the Knight Alzheimer Disease Research Center. ^{11}C-PK11195 standard uptake value ratio (SUVR) and ^{11}C-PiB mean cortical binding potential (MCBP) were used to evaluate neuroinflammation and Aβ deposition in-vivo, respectively. Fluid-attenuated inversion recovery MR images were acquired to obtain baseline WMH volume and its progression over 11.5 years. Composite cognitive scores (global, processing speed and memory) were computed at baseline and follow-up over 7.5 years. Multiple linear regression models evaluated the association between PET biomarkers (^{11}C-PK11195 SUVR and ^{11}C-PiB MCBP) and baseline WMH volume and cognitive function. Moreover, linear mixed-effects models evaluated whether PET biomarkers predicted greater WMH progression or cognitive decline over a decade.
Results: Fifteen participants (62.5%) had mixed AD (positive PiB) and VCID (at least one vascular risk factor) pathologies. Elevated ^{11}C-PK11195 SUVR, but not ^{11}C-PiB MCBP, was associated with greater baseline WMH volume and predicted greater WMH progression. Elevated ^{11}C-PiB MCBP was associated with baseline memory and global cognition. Elevated ^{11}C-PK11195 SUVR and elevated ^{11}C-PiB MCBP independently predicted greater global cognition and processing speed declines. No association was found between ^{11}C-PK11195 SUVR and ^{11}C-PiB MCBP.
Conclusions: Neuroinflammation and Aβ deposition may represent two distinct pathophysiological pathways, and both independently contributed to the progression of cognitive impairment in mixed AD and VCID pathologies. Neuroinflammation, but not Aβ deposition, contributed to WMH volume and progression.

Abbreviations: Aβ, amyloid beta peptides; AD, Alzheimer's disease; CDR, clinical dementia rating; CSVD, cerebral small vessel disease; CRP, C-reactive protein; FCSRT, Free and Cued Selective Reminding Test; FLAIR, fluid-attenuated inversion recovery; GM, cerebral gray matter; MCBP, mean cortical binding potential; MMSE, mini-mental state exam; NAWM, normal appearing white matter; ROI, region of interest; SUVR, standardized uptake value ratio; TSPO, translocator protein; VCID, vascular contributions to cognitive impairment and dementia; WAIS, Wechsler Adult Intelligence Scale; WB, whole brain; WMH, white matter hyperintensities; WMS, Wechsler Memory Scale.

* Corresponding author at: Mallinckrodt Institute of Radiology, Washington University School of Medicine, 510 S Kingshighway, WPAV CCIR, CB 8131, St. Louis, MO 63110, USA.
E-mail address: hongyuan@wustl.edu (H. An).
[1] Co–first authors.

https://doi.org/10.1016/j.nicl.2023.103373
Received 29 October 2022; Received in revised form 18 January 2023; Accepted 8 March 2023
Available online 11 March 2023

1. Introduction

Vascular contributions to cognitive impairment and dementia (VCID) represents a spectrum of underlying pathological processes leading to cerebrovascular brain injury and dementia. Cerebral small vessel disease (CSVD) is the most common contributor to VCID (Gorelick et al., 2011). Vascular risk factors of CSVD include hypertension, hyperlipidemia, diabetes, and smoking (Dickie et al., 2016). On the other hand, Alzheimer's disease (AD) is a progressive neurodegenerative disease caused by the accumulation of amyloid plaques and neurofibrillary tangles. Though the primary putative pathogeneses of these diseases are distinct, AD and VCID pathologies commonly coexist in the community-dwelling elderly (Schneider et al., 2007). Mixed pathology increases the odds of dementia by almost three times. White matter hyperintensities (WMH) of presumed vascular and ischemic origin (Kang et al., 2022) are often found in patients with AD and VCID (Alber et al., 2019; Lee et al., 2016). The pathogenic mechanisms underlying disease risk and progression are not completely understood in mixed AD and VCID.

Amyloid beta peptide (Aβ) aggregates defines a key pathological feature of AD and can be measured using ^{11}C-Pittsburgh compound B (^{11}C-PiB) PET imaging (Cohen and Klunk, 2014). Emerging literature has suggested the role of neuroinflammation in AD and VCID (Werry et al., 2019; Wu et al., 2013). Systemic serum and cerebrospinal fluid markers of inflammation, including C-reactive protein (CRP) and matrix metalloproteinases, are elevated in patients with CSVD (Mitaki et al., 2016; Rosenberg, 2017). Elevated CRP during midlife may promote late-life white matter structural injury and cognitive decline over 20 years (Walker et al., 2019; Walker et al., 2018). PET imaging using ^{11}C-PK11195, a radioligand that binds to the 18 kDa translocator protein (TSPO) located on the membrane of microglia and astrocytes, has also been used to investigate neuroinflammation in patients with AD (Wang et al., 2022) and CSVD (Walsh et al., 2021).

It has been reported that pathologic cerebral Aβ deposition is associated with activated macrophages, microglia and astrocytes as well as the release of pro-inflammatory cytokines in AD (Dorey et al., 2014) and CSVD (Rosenberg, 2017). There is a dearth of literature investigating both neuroinflammation and Aβ aggregation from the same patients in AD and VCID imaging and clinical manifestations. It is not readily discernible whether neuroinflammation and Aβ deposition are distinct or entangled pathophysiological mechanisms in patients with mixed AD and VCID pathologies. In this study, we hypothesized that neuroinflammation, manifesting as elevated ^{11}C-PK11195 standard uptake value ratio (SUVR), is associated with larger WMH volume and predicts greater WMH progression in elderly participants with a range of vascular risk factors. We also hypothesized that neuroinflammation, as an independent pathophysiological process, contributes to cognitive decline in conjunction with elevated Aβ deposition measured by ^{11}C-PiB mean cortical binding potential (MCBP).

2. Methods

2.1. Participant and data acquisition

This study is a retrospective analysis using data from twenty-four elderly participants who underwent ^{11}C-PK11195 PET, ^{11}C-PiB PET, and MRI scans at the Washington University Knight Alzheimer Disease Research Center (ADRC). This study was approved by the Institutional Review Board of Washington University School of Medicine with written informed consent.

^{11}C-PK11195 PET and ^{11}C-PiB PET images were acquired on a Siemens 962 HR + PET scanner (Siemens AG, Knoxville, TN, USA) from all participants between 2004 and 2007. Sixty-minute dynamic PET scans were acquired immediately after the tracer injection (injection dose: 11.0 [8.4, 12.1] mCi for ^{11}C-PK11195 and 10.8 [7.6, 13.0] mCi for ^{11}C-PiB).

Serial MR images were collected between 2004 and 2022. All baseline MRI were acquired on a Siemens 1.5T Vision scanner (Siemens Healthineers, Erlangen, Germany) from 2004 to 2006, and all follow-up MRI were acquired on a Siemens 3T Tim Trio, a 3T Biograph mMR, or a 3T Prisma scanner from 2009 to 2022. T1 magnetization-prepared rapid gradient-echo (MPRAGE) images were acquired from all participants (baseline 1.5T scan parameters: echo time (TE)/repetition time (TR)/inversion time (TI) = 4/9.7/20 ms; follow-up 3T scan parameters: TE/TR/TI = 3.16/2400/1000 ms). Nineteen participants underwent baseline fluid-attenuated inversion recovery (FLAIR) scans, and nine had follow-up FLAIR scans (baseline 1.5T scan parameters: TE/TR/TI = 120/10000/2600 ms; follow-up 3T scan parameters: TE/TR/TI = 76/9000/2500 ms).

The Mini-Mental State Examination (MMSE) and Clinical Dementia Rating (CDR®) scores were collected. Serial cognitive tests were performed using standard Knight ADRC cognitive battery (Johnson et al., 2008) at an approximately 12-month interval between 1987 and 2018. Clinical evaluations were performed by following the ADRC clinical core codebook (https://knightadrc.wustl.edu/wp-content/uploads/2021/07/Clinical-Core-Codebook-UDS2.pdf). The presence of vascular risk factors, including hypertension, hypercholesterolemia, diabetes, stroke or transient ischemic attack, and smoking, were determined by self-reported medical history or by medical chart review. Similar to a previous work (Gottesman et al., 2017), an overall vascular risk score, with 1 point for each risk factor, was calculated. Of note, self-reported stroke may underestimate its true incidence (Day et al., 2020).

The longitudinal study timeline is provided in Fig. 1. Individual participant's ^{11}C-PK11195 PET scan time was used as the timepoint zero. ^{11}C-PiB PET images were acquired at −15.5 [−20, −12.5] months (negative numbers indicate that data was acquired earlier than the ^{11}C-PK11195 PET scan). Baseline MR images were acquired at −9 [−17.5, −6] months. Follow-up MR images were acquired from 9 participants 3 [3, 5] times up to 121 [100, 138] months. The baseline MMSE and CDR scores were collected at 0 [−5, 3] months. Twenty-one participants had follow-up MMSE up to 87 [57, 108] months and follow-up CDR up to 87 [62, 108] months, both at an approximately 12-month interval. The first cognitive data were acquired at −64.5 [−139.2, −31.8] months. The cognitive data closest to the ^{11}C-PK11195 PET scan were acquired at 0 [−2, 4.2] months and used as baseline cognitive data in this study. Beyond the baseline cognitive assessments, twenty-one participants had 7 [5, 9] follow-up cognitive assessments up to 88 [61, 135] months. The baseline clinical evaluation was performed at 2 [−1.2, 5.5] months. Twenty-two participants had follow-up clinical evaluations up to 76.5 [54.5, 88.2] months at an approximately 12-month interval.

2.2. MRI data processing

Baseline and follow-up T1 MPRAGE segmented and parcellated using Freesurfer 5.3 (Martinos Center for Biomedical Imaging, Charlestown, MA, USA), with careful quality control and manual editing with consistent criteria. WMH lesions were delineated manually by a board-certified neurologist (P. Kang) on FLAIR images using Medical Image Processing, Analysis, and Visualization software (https://mipav.cit.nih.gov). FLAIR images and lesion masks were co-registered to T1 MPRAGE images using FMRIB's Linear Image Registration Tool (FLIRT) in the FSL toolbox (Jenkinson et al., 2002). To account for brain volume variation across participants and time, normalized WMH volume was computed as a ratio of WMH volume to brain tissue volume. The brain tissue volume was defined as the summation of cerebral GM and WM volumes. Linear regression was performed between longitudinal WMH volume and age to compute the average annual WMH progression (Table 1).

Baseline FLAIR images and WMH lesion masks were co-registered to the International Consortium for Brain Mapping atlas using Advanced Normalization Tools (Fonov et al., 2009). A WMH lesion density map was then calculated from all 19 participants. A group cumulative WMH region of interest (ROI) was defined in white matter with a lesion density

greater than zero (Fig. 2A, color overlay). A group common normal appearing white matter (NAWM) ROI was defined in white matter with a lesion density of zero (Fig. 2B, blue overlay). Other widely accepted CSVD MRI features, including lacunar infarct, lobar and deep microbleeds, cortical superficial siderosis, and enlarged perivascular spaces were reviewed and summarized in Table 1 (Wardlaw et al., 2013).

2.3. PET data processing

^{11}C-PK11195 and ^{11}C-PiB PET data were reconstructed dynamically using filtered back projection algorithm with 24 × 5-second frames, 9 × 20-second frames, 10 × 1-minute frames, and 9 × 5-minute frames. After inter-frame motion correction, ^{11}C-PK11195 standardized uptake value ratio (SUVR) maps were computed from the 10–60 min frames using the median cerebellar cortex as the reference region. After co-registering to the baseline T1 MPRAGE images using FSL's FLIRT, average ^{11}C-PK11195 SUVR was calculated in the whole brain (WB), cerebral gray matter (GM), WMH and NAWM. A recent study suggested that neuroinflammation in precuneus, posterior cingulate, lateral temporal and inferior parietal cortices had high accuracy in differentiating participants with normal cognition, mild cognitive decline, and AD (Pascoal et al., 2021). Therefore, we also evaluated ^{11}C-PK11195 SUVR in these four cortical regions defined by Freesurfer. ^{11}C-PiB data was processed using a PET Unified Pipeline (https://github.com/ysu001/PUP). The binding potential was determined by Logan plot (Logan et al., 1990) using the frames from 0 to 60 min with the cerebellar cortex as the reference region. Regional spread function-based partial volume correction was performed (Rousset et al., 2008). As a index of Aβ burden, MCBP was calculated by averaging binding potential in the prefrontal cortex, gyrus rectus, lateral temporal, and precuneus regions defined by Freesurfer (Mintun et al., 2006).

2.4. Cognitive data processing

Similar to previous works (Cutter et al., 1999; Wang et al., 2018), the raw scores of each cognitive test were first normalized to z-scores using the group mean and standard deviation of the first cognitive test scores across all participants. Three standardized composite z-scores, zGlobal, zSpeed, and zMemory, were calculated by averaging the z-scores of individual tests. zGlobal was calculated if ≥8 of 11 following tests were available: Wechsler Adult Intelligence Scale (WAIS) Block Design, WAIS Information, Category Fluency (Animals), Wechsler Memory Scale (WMS) Digits Forward, WMS Digits Backward, Boston Naming Test, Trailmaking A, Trailmaking B, WAIS-R Digit Symbol, Associate Memory (WMS Associates Recall (Easy) divided by 2+ WMS Associates Recall (Hard)), and the total free recall score from the Free and Cued Selective Reminding Test (FCSRT). zSpeed was calculated if ≥2 of 3 following tests were available: Trailmaking A, Trailmaking B, and WAIS-R Digit Symbol. zMemory was calculated as an average z-score of two memory tests, Associate Memory and the total free recall score from the FCSRT. Scores for Trailmaking A and B were inverted such that higher scores indicated better performance. Higher composite z-scores indicate better performance. Twenty-two, twenty-two, and twenty-one participants had baseline zGlobal, zSpeed and zMemory scores, respectively. Eighteen participants had 5 [4, 7] follow-up zGlobal scores. Eighteen participants had 5 [4, 7] follow-up zSpeed. Twenty-one participants had 7 [4, 9] follow-up zMemory scores. Linear regression was performed between longitudinal cognitive score and age to compute the average annual cognitive change.

Table 1
Participant characteristics.

	Variables	N = 24[a]
Demographics	Age at the time of ^{11}C-PK11195 Scan	78 [64.8, 83]
	Female	14 (58.3%)
	African American	3 (12.5%)
	Education	16 [12 18]
Vascular risk factors	Hypertension	14 (58.3%)
	Hyperlipidemia	12 (50.0%)
	Diabetes Mellitus	3 (12.5%)
	Stroke or transient ischemic attack	2 (8.3%)
	Smoking	1 (4.2%)
	Participants with at least one vascular risk factor	20 (83.3%)
Imaging characteristics	PiB Positive (^{11}C-PiB MCBP > 0.18)	17 (70.8%)
	Baseline WMH volume (ml)	4.06 [2.14, 19.21]
	Baseline normalized WMH volume	0.52% [0.22%, 2.30%]
	Participants with baseline WMH volume >1 ml	17/19 (89.5%)
	WMH volume progression rate (ml per year)[b]	0.23 [0.12, 0.42]
	Normalized WMH volume progression rate (per year)[b]	0.03% [0.02%, 0.04%]
	Lacunar infarct	2/21 (9.5%)
	Lobar microbleeds	1/12 (8.3%)
	Deep microbleeds	1/12 (8.3%)
	Cortical superficial siderosis	1/12 (8.3%)
	Enlarged perivascular spaces	9/15 (60%)
Baseline cognitive and functional status	MMSE	28.5 [26.8 30]
	Participants with MMSE ≥ 24	21 (87.5%)
	CDR	0 [0, 0.5]
	Participants with CDR = 0	17 (70.8%)

[a] Values are shown as Median [Interquartile range] or numbers (%).
[b] N = 9.

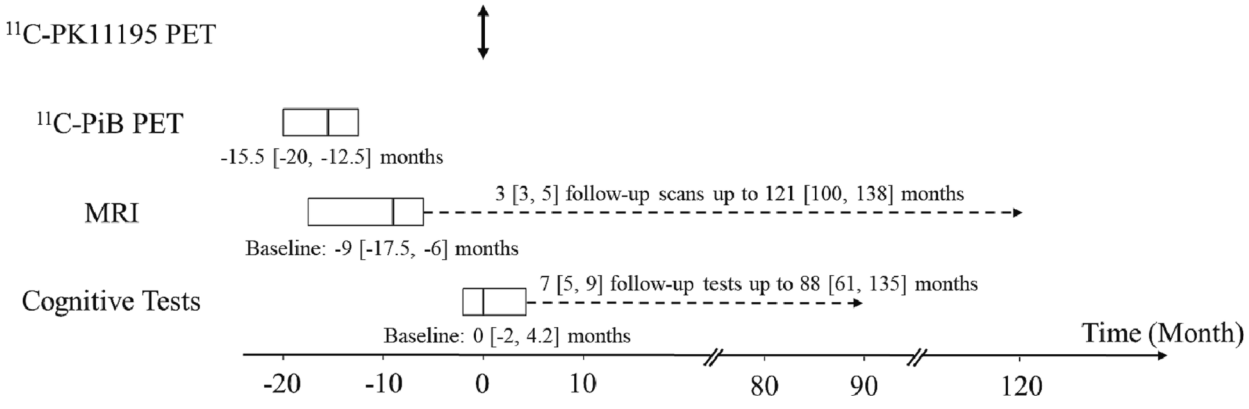

Fig. 1. Longitudinal study timeline. Timepoint zero was defined by individual participant's ^{11}C-PK11195 PET scan.

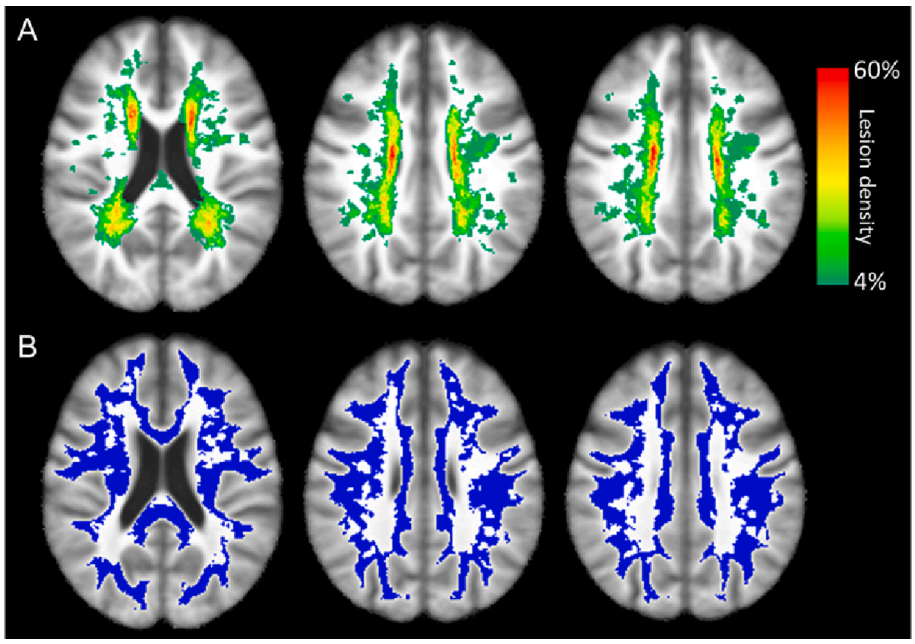

Fig. 2. Baseline WMH lesion density map (A) and group common NAWM ROI (B, marked in blue). (For interpretation of the references to color in this figure legend, the reader is referred to the web version of this article.)

2.5. Statistical analysis

Statistical analyses were performed using R 3.6.1 (Foundation for Statistical Computing, Vienna, Austria). Two-tailed significance was set to 0.05 *a priori*. All models were evaluated for multicollinearity using variance inflation factors (VIF).

To evaluate the association between PET imaging biomarkers of neuroinflammation (regional ^{11}C-PK11195 SUVR) and Aβ deposition (^{11}C-PiB MCBP) and baseline normalized WMH volume and cognitive function, multiple linear regression models controlling for the time difference between PET and baseline MR scans or baseline cognitive test were utilized. In addition to PET imaging biomarkers, we also evaluated the possible entry of age, sex, education, and vascular risk score into these models. For the continuous variables such as age, vascular risk score, and education, Pearson correlation between an independent variable and the dependent variable (baseline WMH volume or cognitive function) was used to determine its entry into the multi-variable models. The entry of the categorical variable sex was determined by whether the dependent variable was different between males and females using a *t*-test. A univariate $P < 0.2$ was required for entry into the multiple linear regression model. The multiple linear regression models used in this study are summarized in Table 2 and Table 4. We also evaluated whether regional ^{11}C-PK11195 SUVR was associated with ^{11}C-PiB MCBP using multiple linear regression controlling for age and time difference between the two acquisitions.

Linear mixed-effects models with an intercept only random effect for participant, controlling for sex, education, and vascular risk score were used to evaluate whether PET imaging biomarkers predicted greater WMH progression and cognitive decline. Normalized WMH volumes or cognitive scores acquired at baseline and all follow-up visits were included in these longitudinal analyses. The mixed-effects models are summarized in Table 3 and Table 5. Models were assessed for normality quantitatively with the Shapiro-Wilk and Anderson-Darling tests and graphically using the histogram and QQ-plot of model residuals. The interaction between regional ^{11}C-PK11195 SUVR and age and the interaction between ^{11}C-PiB MCBP and age were investigated as the primary independent variables.

Table 2
Multiple linear regression models between baseline WMH volume and PET biomarkers.

Model: Baseline WMH volume ~ Regional ^{11}C-PK11195 SUVR + Age + Vascular Risk Score	
PK Region[a]	**PK SUVR**[b]
Whole Brain ROI	**0.281 [0.008, 0.555]** *
NAWM ROI	0.197 [−0.060, 0.454]
WMH ROI	NA[c]
Cerebral Gray Matter ROI	**0.240 [0.018, 0.462]** *
Precuneus ROI	0.117 [−0.066, 0.300]
Posterior Cingulate ROI	0.086 [−0.040, 0.212]
Lateral Temporal Cortex ROI	NA[c]
Inferior Parietal Cortex ROI	NA[c]

*$P < 0.05$.
[a] Each row presents results from a separate model evaluating the effect of ^{11}C-PK11195 SUVR in a specific region.
[b] Values are shown as beta coefficient [95% confidence internal].
[c] Not included in the multiple linear regression model because $P > 0.2$ in the univariate test.

3. Results

3.1. Participant characteristics

Participant characteristics are summarized in Table 1. Twenty participants (83.3%) had at least one vascular risk factor. Seventeen participants (70.8%) were PiB positive (^{11}C-PiB MCBP > 0.18) (Mintun et al., 2006). Fifteen participants (62.5%) had both a positive PiB scan and at least one vascular risk factor. The baseline WMH volume was 4.06 [2.14, 19.21] ml, corresponding to normalized WMH volume of 0.52% [0.22%, 2.30%]. Seventeen of nineteen participants (89.5%) had >1 ml WMH volume. Enlarged perivascular spaces were found in 60% of participants, while lacunar infarct, microbleeds, and cortical superficial siderosis were less frequent at baseline. Among participants with follow-up clinical evaluations (N = 22), one, three, and two participants developed hypertension, hyperlipidemia, Diabetes Mellitus, respectively. One participant became a smoker. Twenty-one (87.5%) and seventeen (70.8%) participants had normal baseline MMSE (>=24) and

Table 3
Longitudinal prediction of WMH progression using mixed-effects models with a random effect for participant.

Model: WMH volume ~ Regional ^{11}C-PK11195 SUVR × Age + ^{11}C-PiB MCBP × Age + Sex + Vascular Risk Score		
PK Region[a]	**PK SUVR × Age**[b]	**PiB MCBP × Age**[b]
Whole Brain ROI	**0.030 [0.004, 0.054] ***	−0.001 [−0.002, 0.001]
NAWM ROI	0.014 [−0.004, 0.033]	−0.000 [−0.002, 0.001]
WMH ROI	−0.004 [−0.018, 0.010]	−0.001 [−0.003, 0.001]
Cerebral Gray Matter ROI	**0.027 [0.010, 0.044] ****	−0.000 [−0.002, 0.001]
Precuneus ROI	**0.013 [0.002, 0.024] ***	−0.001 [−0.003, 0.000]
Posterior Cingulate ROI	0.009 [−0.000, 0.017]	−0.001 [−0.002, 0.001]
Lateral Temporal Cortex ROI	0.012 [−0.002, 0.027]	−0.000 [−0.002, 0.002]
Inferior Parietal Cortex ROI	0.006 [−0.004, 0.016]	−0.001 [−0.003, 0.001]

*$P < 0.05$.
**P < 0.01.
[a] Each row presents results from a separate model evaluating the effect of ^{11}C-PK11195 SUVR in a specific region.
[b] Values are shown as beta coefficient [95% confidence internal].

CDR (=0), respectively (Lezak et al., 2004). Among participants with follow-up CDR (N = 21), eight participants had CDR progression from 0 to 0.5 (N = 1), from 0 to 1 (N = 3), from 0 to 2 (N = 3), and from 0.5 to 2 (N = 1). Thirteen participants had no change (CDR = 0: N = 10, CDR = 0.5: N = 3). Among participants with follow-up MMSE (N = 21), four participants progressed from normal MMSE (>=24) to abnormal MMSE (<24). As shown in Table 1, this study cohort has a wide presence of mixed AD and VCID pathologies. The baseline WMH lesion density map and group common NAWM ROI are shown in Fig. 2. WMH lesion density was the highest in the periventricular and deep white matter regions, consistent with previous findings (Kang et al., 2022).

3.2. Association between PET biomarkers and baseline and longitudinal WMH volume

Fig. 3 shows baseline FLAIR images and PET ^{11}C-PK11195 SUVR maps from two representative participants with WMH volumes of 1.89 ml (Fig. 3A) and 45.44 ml (Fig. 3B). The WB ^{11}C-PK11195 SUVR were 0.94 (Fig. 3C) and 1.07 (Fig. 3D), respectively. The multiple linear regression between PET imaging markers and WMH volume is summarized in Table 2. ^{11}C-PiB MCBP did not meet the criteria for entering the multiple linear regression model. ^{11}C-PK11195 SUVR in WB ($\beta = 0.281$, $P = 0.044$) and GM ($\beta = 0.240$, $P = 0.036$) were associated with WMH volume after controlling for age and vascular risk score.

The longitudinal progression of WMH is demonstrated in Fig. 4A. WHM volume increased by 0.23 [0.12, 0.42] ml per year, corresponding to normalized WMH volume of 0.03% [0.02%, 0.04%] per year over 11.5 years (Fig. 4A). The association between PET biomarkers and longitudinal WMH progression is summarized in Table 3. Elevated WB ^{11}C-PK11195 SUVR together with age ($\beta = 0.030$, $P = 0.027$), elevated GM ^{11}C-PK11195 SUVR together with age ($\beta = 0.027$, $P = 0.004$) and elevated precuneus ^{11}C-PK11195 SUVR together with age ($\beta = 0.013$, $P = 0.028$) respectively predicted greater WMH progression, while elevated ^{11}C-PiB MCBP together with age did not.

VIFs were smaller than 2.1 for all independent variables in all baseline and longitudinal models, demonstrating no multicollinearity in the analyses.

Table 4
Multiple linear regression models between baseline cognitive function and PET biomarkers.

Model: Baseline zGlobal ~ Regional ^{11}C-PK11195 SUVR + ^{11}C-PiB MCBP + Age + Education + Vascular Risk Score		
PK Region[a]	**PK SUVR**[b]	**PiB MCBP**[b]
Whole Brain ROI	−0.287 [−10.388, 9.813]	**−0.568 [−1.032, −0.103] ***
NAWM ROI	1.267 [−7.696, 10.231]	**−0.589 [−1.050, −0.128] ***
WMH ROI		
Cerebral Gray Matter ROI		
Precuneus ROI		
Posterior Cingulate ROI	NA[c]	**−0.569 [−0.993, −0.144] ***
Lateral Temporal Cortex ROI		
Inferior Parietal Cortex ROI		
Model: Baseline zSpeed ~ Regional ^{11}C-PK11195 SUVR + Age + Education + Vascular Risk Score		
PK Region[a]	**PK SUVR**[b]	
Whole Brain ROI	−5.873 [−21.245, 9.499]	
NAWM ROI	−3.533 [−17.378, 10.312]	
WMH ROI	NA[c]	
Cerebral Gray Matter ROI	−5.351 [−18.828, 8.126]	
Precuneus ROI		
Posterior Cingulate ROI	NA[c]	
Lateral Temporal Cortex ROI		
Inferior Parietal Cortex ROI		
Model: Baseline zMemory ~ Regional ^{11}C-PK11195 SUVR + PiB MCBP + Age		
PK Region[a]	**PK SUVR**[b]	**PiB MCBP**[b]
Whole Brain ROI	−5.075 [−16.009, 5.859]	**−0.798 [−1.327, −0.268] ****
NAWM ROI	−3.550 [−13.990, 6.889]	**−0.804 [−1.343, −0.266] ****
WMH ROI		
Cerebral Gray Matter ROI		
Precuneus ROI		
Posterior Cingulate ROI	NA[c]	**−0.818 [−1.360, −0.276] ****
Lateral Temporal Cortex ROI		
Inferior Parietal Cortex ROI		

*$P < 0.05$.
**P < 0.01.
[a] Each row presents results from a separate model evaluating the effect of ^{11}C-PK11195 SUVR in a specific.
[b] Values are shown as beta coefficient [95% confidence internal].
[c] Not included in the multiple linear regression model because P > 0.2 in the univariate test.

3.3. Association between PET biomarkers and baseline and longitudinal cognition

The multiple linear regression between PET biomarkers and baseline cognitive function is summarized in Table 4. ^{11}C-PiB MCBP but not ^{11}C-PK11195 SUVR was associated with baseline zGlobal ($P < 0.05$) and zMemory ($P < 0.01$) in multiple linear regression models. Neither regional ^{11}C-PK11195 SUVR nor ^{11}C-PiB MCBP was associated with baseline zSpeed.

The longitudinal decline of cognitive function is demonstrated in Fig. 4 (B-D). Global, processing speed and memory function decreased

Table 5
Longitudinal prediction of cognitive decline using mixed-effects models with a random effect for participant.

Model: zGlobal ~ Regional ^{11}C-PK11195 SUVR × Age + ^{11}C-PiB MCBP × Age + Sex + Education + Vascular Risk Score		
PK Region[a]	**PK SUVR × Age**[b]	**PiB MCBP × Age**[b]
Whole Brain ROI	−0.840 [−2.302, 0.622]	**−0.155 [−0.222, −0.088]** ***
NAWM ROI	−0.491 [−1.780, 0.798]	**−0.153 [−0.230, −0.077]** ***
WMH ROI	−0.228 [−1.002, 0.546]	**−0.163 [−0.230, −0.097]** ***
Cerebral Gray Matter ROI	−0.461 [−1.453, 0.530]	**−0.172 [−0.236, −0.108]** ***
Precuneus ROI	**−0.629 [−1.249, −0.008]** *	**−0.164 [−0.227, −0.100]** ***
Posterior Cingulate ROI	0.301 [−0.238, 0.840]	**−0.171 [−0.234, −0.107]** ***
Lateral Temporal Cortex ROI	**−0.959 [−1.866, −0.052]** *	**−0.184 [−0.249, −0.119]** ***
Inferior Parietal Cortex ROI	**−0.958 [−1.498, −0.419]** ***	**−0.161 [−0.222, −0.101]** ***
Model: zSpeed ~ Regional ^{11}C-PK11195 SUVR × Age + ^{11}C-PiB MCBP × Age + Sex + Education + Vascular Risk Score		
PK Region[a]	**PK SUVR × Age**[b]	**PiB MCBP × Age**[b]
Whole Brain ROI	**−2.512 [−4.621, −0.404]** *	**−0.253 [−0.361, −0.146]** ***
NAWM ROI	**−2.100 [−3.627, −0.572]** **	**−0.239 [−0.352, −0.126]** ***
WMH ROI	−1.062 [−2.224, 0.100]	**−0.282 [−0.388, −0.177]** ***
Cerebral Gray Matter ROI	−1.106 [−2.738, 0.526]	**−0.291 [−0.396, −0.186]** ***
Precuneus ROI	−0.809 [−1.788, 0.169]	**−0.275 [−0.382, −0.168]** ***
Posterior Cingulate ROI	−0.025 [−0.847, 0.798]	**−0.308 [−0.414, −0.202]** ***
Lateral Temporal Cortex ROI	**−1.770 [−3.122, −0.418]** *	**−0.316 [−0.420, −0.212]** ***
Inferior Parietal Cortex ROI	**−1.200 [−2.062, −0.337]** **	**−0.254 [−0.356, −0.153]** ***
Model: zMemory ~ Regional ^{11}C-PK11195 SUVR × Age + ^{11}C-PiB MCBP × Age + Sex + Education + Vascular Risk Score		
PK Region[a]	**PK SUVR × Age**[b]	**PiB MCBP × Age**[b]
Whole Brain ROI	−0.753 [−2.284, 0.777]	−0.010 [−0.077, 0.058]
NAWM ROI	−0.391 [−1.632, 0.850]	−0.002 [−0.077, 0.073]
WMH ROI	−0.222 [−1.029, 0.584]	−0.001 [−0.069, 0.067]
Cerebral Gray Matter ROI	−0.524 [−1.673, 0.626]	−0.035 [−0.112, 0.042]
Precuneus ROI	−0.543 [−1.263, 0.177]	−0.049 [−0.127, 0.029]
Posterior Cingulate ROI	0.194 [−0.372, 0.760]	−0.034 [−0.111, 0.042]
Lateral Temporal Cortex ROI	−0.685 [−1.657, 0.286]	−0.038 [−0.115, 0.040]
Inferior Parietal Cortex ROI	**−1.029 [−1.653, −0.405]** **	−0.054 [−0.126, 0.018]

*$P < 0.05$.
**P < 0.01.
***P < 0.001.
[a] Each row presents results from a separate model evaluating the effect of ^{11}C-PK11195 SUVR in a specific region.
[b] Values are shown as beta coefficient [95% confidence interval].

by 0.10 [0.01 0.32], 0.15 [0.02, 0.59], and 0.07 [0.02, 0.30] per year over 7.5 years, respectively (Fig. 4(B-D)). The associations between PET biomarkers and longitudinal cognitive decline are summarized in Table 5. Elevated precuneus ^{11}C-PK11195 SUVR together with age (β = -0.629, $P = 0.050$), elevated lateral temporal cortex ^{11}C-PK11195 SUVR together with age ($\beta = -0.959$, $P = 0.041$), and elevated inferior parietal cortex ^{11}C-PK11195 SUVR together with age ($\beta = -0.958$, $P < 0.001$), respectively, predicted greater zGlobal decline independent of ^{11}C-PiB MCBP together with age ($P < 0.001$). Elevated WB ^{11}C-PK11195 SUVR

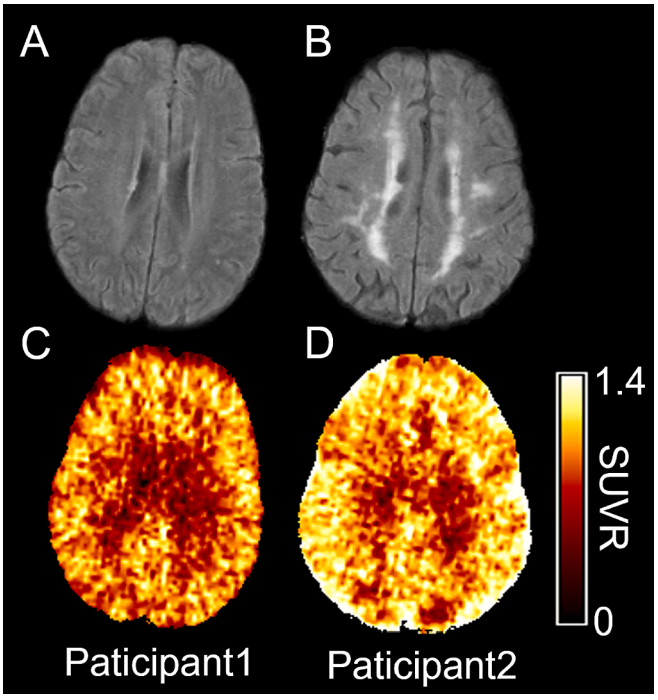

Fig. 3. Baseline MR FLAIR images (A, B) and PET ^{11}C-PK11195 SUVR maps (C, D) from two representative participants. WMH volumes were 1.89 ml and 45.44 ml, and the whole brain ^{11}C-PK11195 SUVR were 0.94 and 1.07 in Participant 1 and Participant 2, respectively. ^{11}C-PK11195 SUVR was higher in participants with larger WMH volume.

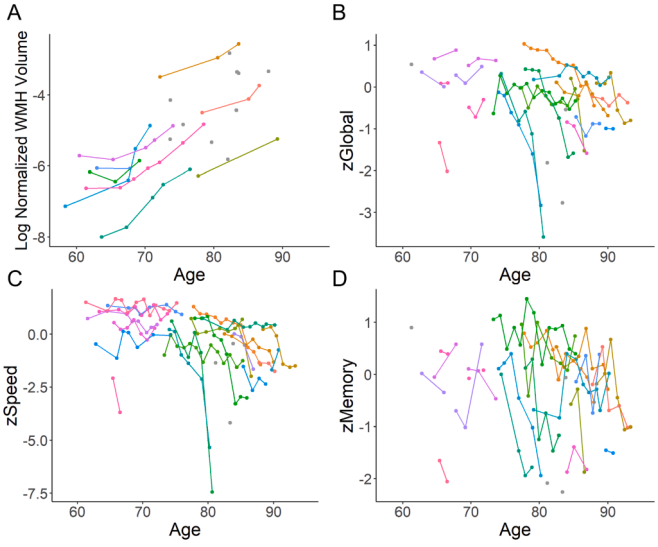

Fig. 4. Longitudinal WMH progression (A) and cognitive decline (B-D). Different colors indicate data from different participants. Solitary gray circles indicate participants who had only one baseline measurement. Normalized WMH volume increased by 0.03% [0.02%, 0.04%] per year over 11.5 years **(A).** Global, processing speed and memory function decreased by 0.10 [0.01 0.32], 0.15 [0.02, 0.59], and 0.07 [0.02, 0.30] per year over 7.5 years, respectively **(B-D)**.

together with age ($\beta = -2.512$, $P = 0.021$), elevated NAWM ^{11}C-PK11195 SUVR together with age ($\beta = -2.100$, $P = 0.008$), elevated lateral temporal cortex ^{11}C-PK11195 SUVR together with age ($\beta = -1.770$, $P = 0.011$), and elevated inferior parietal cortex ^{11}C-PK11195 SUVR together with age ($\beta = -1.200$, $P = 0.007$), respectively predicted greater zSpeed decline independent of ^{11}C-PiB MCBP together with age

($P < 0.001$). Elevated ^{11}C-PK11195 SUVR in inferior parietal cortex together with age ($\beta = -1.029$, $P = 0.002$) predicted greater zMemory decline independent from ^{11}C-PiB MCBP together with age ($P = 0.145$).

VIF was <2.7 for independent variables in all baseline and longitudinal models, demonstrating no multicollinearity in the analyses.

3.4. Association between ^{11}C-PK11195 SUVR and ^{11}C-PiB MCBP

Fig. 5 shows scatter plots of ^{11}C-PK11195 SUVR from various ROIs and ^{11}C-PiB BP in the MC ROI (MCBP). Regional ^{11}C-PK11195 SUVR was not associated with ^{11}C-PiB MCBP. Notable, ^{11}C-PK11195 SUVR was not correlated with ^{11}C-PiB in the same MC region (Fig. 5D).

4. Discussion

Neuroinflammation is emerging as an important pathomechanism in AD and VCID, and may have direct implications in the development of potential therapeutics. Chronic inflammation may result in a pathologic cascade, ultimately resulting in inappropriate inflammatory infiltration and tissue destruction. Post-mortem studies show inflammatory changes such as microgliosis and astrogliosis in patients with vascular cognitive impairment in the late stages of CSVD (Gouw et al., 2011; van Veluw et al., 2022). Low et al. found neuroinflammation, measured by regional ^{11}C-PK11195 binding was associated with various CSVD markers in a cohort of participants consisting of healthy controls, mild AD patients, and amyloid-positive MCI patients (Low et al., 2021). Malpetti et al. demonstrated that elevated anterior temporal ^{11}C-PK11195 binding predicts cognitive decline in patients with symptomatic Alzheimer's disease pathology (Malpetti et al., 2020). While several large-cohort studies have shown an association between systemic inflammatory biomarkers and white matter injury or cognitive decline over 20 to 30 years (Walker et al., 2019; Walker et al., 2018), other studies did not find this association (Metti et al., 2014; Weuve et al., 2006). These mixed findings are likely owing to differences in age, vascular risk factors, disease severity, inflammatory markers investigated, and possible heterogeneity in disease mechanisms (Ridker, 2004). Our study used ^{11}C-PK11195 PET to measure regional neuroinflammation directly, which is more specific than the systemic inflammatory markers. We found elevated ^{11}C-PK11195 SUVR across the whole brain in participants with higher WMH volume, suggesting widespread neuroinflammation.

AD and VCID pathologies commonly coexist in elderly patients with cognitive impairments (Schneider et al., 2007). Post-mortem studies show CSVD pathology in autopsy-confirmed AD (Bangen et al., 2015). It is exceedingly difficult to clinically differentiate between AD and VCID pathomechanisms (Cipollini et al., 2019; Rosenberg et al., 2019). It is crucial that we understand the extent to which AD and VCID pathomechanisms contribute toward the neuroimaging manifestations and cognitive impairment in a personalized manner as targeted therapeutics are developed (Cipollini et al., 2019; Rosenberg et al., 2019). We investigated the roles of neuroinflammation and Aβ deposition in the progression of WMH and cognitive decline in participants with a range of vascular risk factors and Aβ deposition. Neuroinflammation, but not pathologic Aβ deposition, was associated with baseline WMH volume and predicted its progression over 11.5 years. Our results suggest that neuroinflammation is closely linked with imaging abnormalities in patients with mixed AD and VCID pathologies. Moreover, Aβ deposition, but not neuroinflammation, was associated with baseline global cognitive and memory dysfunctions. Both neuroinflammation and Aβ deposition independently predicted cognitive decline over 7.5 years after controlling for age, education, and vascular risk factors. Notably, there was no association between ^{11}C-PK11195 SUVR and ^{11}C-PiB MCBP. Taken together, our findings suggest that neuroinflammation and pathologic Aβ deposition represent distinct pathophysiological mechanisms, and both contribute to disease progression in AD and VCID mixed etiology cognitive impairment. We did not find an association between neuroinflammation and Aβ deposition, suggesting that these two processes act independently from each other in disease progression. Immunohistochemical studies in post-mortem brains from AD patients show that although clustered microglial cells can be observed in and around Aβ plaques, the presence of activated microglia is not consistently associated with Aβ deposition (Haga et al., 1989; Streit, 2005). On the other hand, in-vivo PET studies show positive (Dani et al., 2018), negative (Yokokura et al., 2011) or no (Kreisl et al., 2016) association between neuroinflammation and Aβ deposition in AD or mild cognitive impairment. Of note, these studies focused on AD pathology and did not investigate potential vascular-related risk factors and pathologies. Our findings support the independent roles of neuroinflammation and pathological Aβ deposition in mixed AD and VCID.

Our study has several limitations. Firstly, the sample size of this study was relatively small ($N = 24$). Moreover, only nine participants had longitudinal FLAIR scans, and only 21 participants had longitudinal cognitive data. Secondly, ^{11}C-PK11195, which is a first-generation PET tracer to measure neuroinflammation, has a low signal-to-noise ratio and high non-specific binding (Chauveau et al., 2008). Notably, we did not find an association between NAWM or WMH ^{11}C-PK11195 SUVR and WMH lesion progression, which may be partially due to the low signal-to-noise ratio in white matter. The second- and third-generation TSPO tracers have improved specific binding but suffer large inter-individual variability in binding affinity due to TSPO genetic polymorphisms (Owen et al., 2011). More recently, PET tracers binding to

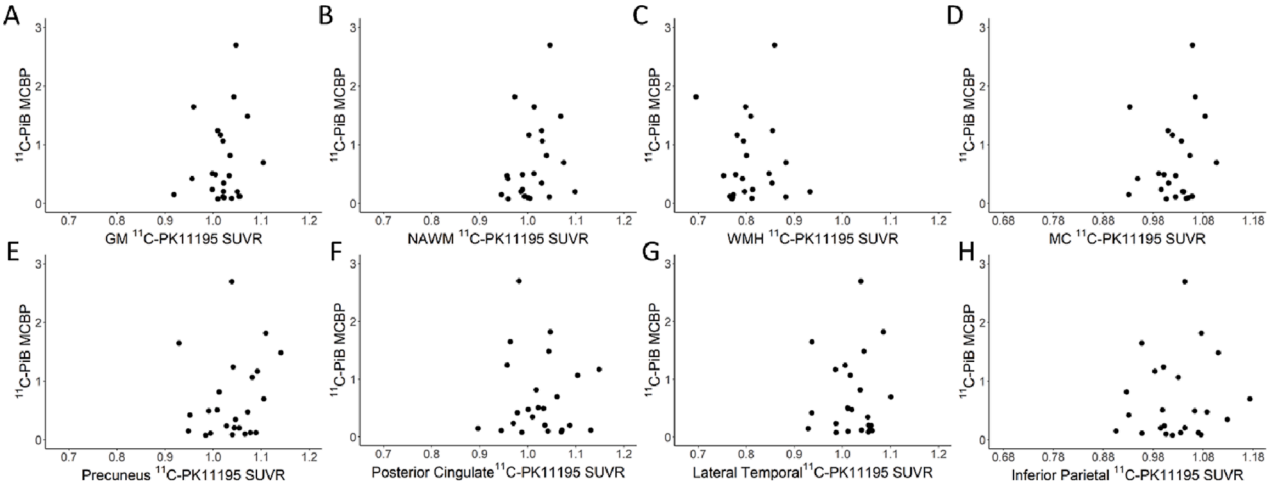

Fig. 5. Scatter plots between regional ^{11}C-PK11195 SUVR and ^{11}C-PiB MCBP. ^{11}C-PK11195 SUVR was not associated with ^{11}C-PiB MCBP in all regions.

other targets involved in neuroinflammatory response beyond TSPO have been developed. For example, ^{11}C-CS1P1 is a tracer targeting sphingosine-1-phosphate receptor subtype 1, a cell membrane G-protein coupled receptor that plays an essential signaling role in the inflammatory response (Jiang et al., 2021). Thirdly, the baseline MRI was acquired using a 1.5T scanner while the follow-up MRI was acquired using a 3T scanner. The use of 1.5T scanner for baseline and 3T scanner at follow-up scans was not ideal but inevitable for a longitudinal study over more than a decade since MRI scanners might be upgraded over the course of the study. The FLAIR imaging protocols are the same for all the 3T scans. The WMH lesions were manually delineated by a board-certified neurologist. It is possible that the WMH obtained at baseline and follow-up may be affected by the use of two different MR fields. We expect small variations for all the 3T images despite three different 3T MR scanner models being used. Finally, the usage of different Freesurfer versions and pipelines may lead to different segmentation results, especially in small cortical ROIs. Due to low signal-to-noise ratio in the ^{11}C-PK11195 PET, results in small ROIs need to be interpreted with caution. Future prospective studies with a larger sample size and using improved tracers are needed to further elucidate neuroinflammation's role in mixed etiology dementia and aim for the development of relevant therapeutics.

5. Conclusions

In conclusion, we demonstrate that neuroinflammation and Aβ deposition represent two distinct pathophysiological pathways in a cohort of elderly participants with mixed AD and VCID pathologies. Neuroinflammation plays a role in the development of WMH early in the course of the disease. Both neuroinflammation and Aβ deposition independently contribute to the progression of cognitive impairments.

Funding

This work was supported by grants from the National Institutes of Health (NIH): P01AG026276 (J.C.M.), P01AG003991 (J.C.M.), P30AG066444 (J.C.M.), 1R01AG054567 (T.L.B.), R01HL129241 (A.L. F.), 1R01NS082561 (H.A.), 1P30NS098577 (Imaging Core, H.A.), RF1NS116565 (H.A. and A.L.F.), R21NS127425 (H.A.), R01NS085419 (J.M.L.), U24NS107230 (J.M.L.), KL2TR002346 (P.K.), R03AG072375 (Q.W.) and R01AG074909 (Q.W.). Additional support was generously provided by the Charles and Joanne Knight Alzheimer's Research Initiative and by the Fred Simmons and Olga Mohan Fund and the Paula and Rodger Riney Funding.

CRediT authorship contribution statement

Chunwei Ying: Data curation, Investigation, Methodology, Software, Visualization, Writing – original draft. **Peter Kang:** Investigation, Methodology, Writing – original draft. **Michael M. Binkley:** Investigation, Visualization, Writing – review & editing. **Andria L. Ford:** Investigation, Writing – review & editing. **Yasheng Chen:** Investigation, Writing – review & editing. **Jason Hassenstab:** Investigation, Writing – review & editing. **Qing Wang:** Writing – review & editing. **Jeremy Strain:** Writing – review & editing. **John C. Morris:** Writing – review & editing. **Jin-Moo Lee:** Writing – review & editing. **Tammie L.S. Benzinger:** Conceptualization, Writing – review & editing. **Hongyu An:** Conceptualization, Funding acquisition, Project administration, Supervision, Writing – original draft.

Declaration of Competing Interest

The authors declare that they have no known competing financial interests or personal relationships that could have appeared to influence the work reported in this paper.

Data availability

Data will be made available on request.

Acknowledgements

We thank Jon Christensen for his help in data processing.

References

Alber, J., Alladi, S., Bae, H.-J., Barton, D.A., Beckett, L.A., Bell, J.M., Berman, S.E., Biessels, G.J., Black, S.E., Bos, I., Bowman, G.L., Brai, E., Brickman, A.M., Callahan, B.L., Corriveau, R.A., Fossati, S., Gottesman, R.F., Gustafson, D.R., Hachinski, V., Hayden, K.M., Helman, A.M., Hughes, T.M., Isaacs, J.D., Jefferson, A. L., Johnson, S.C., Kapasi, A., Kern, S., Kwon, J.C., Kukolja, J., Lee, A., Lockhart, S.N., Murray, A., Osborn, K.E., Power, M.C., Price, B.R., Rhodius-Meester, H.F.M., Rondeau, J.A., Rosen, A.C., Rosene, D.L., Schneider, J.A., Scholtzova, H., Shaaban, C.E., Silva, N.C.B.S., Snyder, H.M., Swardfager, W., Troen, A.M., Veluw, S. J., Vemuri, P., Wallin, A., Wellington, C., Wilcock, D.M., Xie, S.X., Hainsworth, A.H., 2019. White matter hyperintensities in vascular contributions to cognitive impairment and dementia (VCID): knowledge gaps and opportunities. Alzheimer's Dement.: Transl. Res. Clin. Intervent. 5 (1), 107–117.

Bangen, K.J., Nation, D.A., Delano-Wood, L., Weissberger, G.H., Hansen, L.A., Galasko, D.R., Salmon, D.P., Bondi, M.W., 2015. Aggregate effects of vascular risk factors on cerebrovascular changes in autopsy-confirmed Alzheimer's disease. Alzheimers Dement. 11 (4), 394.

Chauveau, F., Boutin, H., Van Camp, N., Dollé, F., Tavitian, B., 2008. Nuclear imaging of neuroinflammation: a comprehensive review of [11 C] PK11195 challengers. Eur. J. Nucl. Med. Mol. Imaging 35 (12), 2304–2319.

Cipollini, V., Troili, F., Giubilei, F., 2019. Emerging biomarkers in vascular cognitive impairment and dementia: from pathophysiological pathways to clinical application. Int. J. Mol. Sci. 20 (11), 2812.

Cohen, A.D., Klunk, W.E., 2014. Early detection of Alzheimer's disease using PiB and FDG PET. Neurobiol. Dis. 72, 117–122.

Cutter, G.R., Baier, M.L., Rudick, R.A., Cookfair, D.L., Fischer, J.S., Petkau, J., Syndulko, K., Weinshenker, B.G., Antel, J.P., Confavreux, C., 1999. Development of a multiple sclerosis functional composite as a clinical trial outcome measure. Brain 122, 871–882.

Dani, M., Wood, M., Mizoguchi, R., Fan, Z., Walker, Z., Morgan, R., Hinz, R., Biju, M., Kuruvilla, T., Brooks, D.J., 2018. Microglial activation correlates in vivo with both tau and amyloid in Alzheimer's disease. Brain 141, 2740–2754.

Day, G.S., Long, A., Morris, J.C., 2020. Assessing the reliability of reported medical history in older adults. J. Alzheimers Dis. 78 (2), 643–652.

Dickie, D.A., Ritchie, S.J., Cox, S.R., Sakka, E., Royle, N.A., Aribisala, B.S., Valdés Hernández, M.D.C., Maniega, S.M., Pattie, A., Corley, J., Starr, J.M., Bastin, M.E., Deary, I.J., Wardlaw, J.M., 2016. Vascular risk factors and progression of white matter hyperintensities in the Lothian Birth Cohort 1936. Neurobiol. Aging 42, 116–123.

Dorey, E., Chang, N., Liu, Q.Y., Yang, Z., Zhang, W., 2014. Apolipoprotein E, amyloid-beta, and neuroinflammation in Alzheimer's disease. Neurosci. Bull. 30 (2), 317–330.

Fonov, V.S., Evans, A.C., McKinstry, R.C., Almli, C.R., Collins, D.L., 2009. Unbiased nonlinear average age-appropriate brain templates from birth to adulthood. Neuroimage 47, S102.

Gorelick, P.B., Scuteri, A., Black, S.E., Decarli, C., Greenberg, S.M., Iadecola, C., Launer, L.J., Laurent, S., Lopez, O.L., Nyenhuis, D., Petersen, R.C., Schneider, J.A., Tzourio, C., Arnett, D.K., Bennett, D.A., Chui, H.C., Higashida, R.T., Lindquist, R., Nilsson, P. M., Roman, G.C., Sellke, F.W., Seshadri, S., American Heart Association Stroke Council, C.o.E., Prevention, C.o.C.N.C.o.C.R., Intervention, Council on Cardiovascular, S., Anesthesia, 2011. Vascular contributions to cognitive impairment and dementia: a statement for healthcare professionals from the American heart association/American stroke association. Stroke 42, 2672-2713.

Gottesman, R.F., Schneider, A.L., Zhou, Y., Coresh, J., Green, E., Gupta, N., Knopman, D. S., Mintz, A., Rahmim, A., Sharrett, A.R., Wagenknecht, L.E., Wong, D.F., Mosley, T. H., 2017. Association between midlife vascular risk factors and estimated brain amyloid deposition. JAMA 317, 1443–1450.

Gouw, A.A., Seewann, A., van der Flier, W.M., Barkhof, F., Rozemuller, A.M., Scheltens, P., Geurts, J.J.G., 2011. Heterogeneity of small vessel disease: a systematic review of MRI and histopathology correlations. J. Neurol. Neurosurg. Psychiatry 82 (2), 126–135.

Haga, S., Akai, K., Ishii, T., 1989. Demonstration of microglial cells in and around senile (neuritic) plaques in the Alzheimer brain. an immunohistochemical study using a novel monoclonal antibody. Acta Neuropathol. 77 (6), 569–575.

Jenkinson, M., Bannister, P., Brady, M., Smith, S., 2002. Improved optimization for the robust and accurate linear registration and motion correction of brain images. Neuroimage 17 (2), 825–841.

Jiang, H., Joshi, S., Liu, H., Mansor, S., Qiu, L., Zhao, H., Whitehead, T., Gropler, R.J., Wu, G.F., Cross, A.H., Benzinger, T.L.S., Shoghi, K.I., Perlmutter, J.S., Tu, Z., 2021. Vitro and in vivo investigation of S1PR1 expression in the central nervous system using [(3)H]CS1P1 and [(11)C]CS1P1. ACS Chem. Neurosci. 12 (19), 3733–3744.

Johnson, D.K., Storandt, M., Morris, J.C., Langford, Z.D., Galvin, J.E., 2008. Cognitive profiles in dementia: Alzheimer disease vs healthy brain aging. Neurology 71 (22), 1783–1789.

Kang, P., Ying, C., Chen, Y., Ford, A.L., An, H., Lee, J.-M., 2022. Oxygen metabolic stress and white matter injury in patients with cerebral small vessel disease. Stroke 53 (5), 1570–1579.
Kreisl, W.C., Lyoo, C.H., Liow, J.-S., Wei, M., Snow, J., Page, E., Jenko, K.J., Morse, C.L., Zoghbi, S.S., Pike, V.W., Turner, R.S., Innis, R.B., 2016. 11C-PBR28 binding to translocator protein increases with progression of Alzheimer's disease. Neurobiol. Aging 44, 53–61.
Lee, S., Viqar, F., Zimmerman, M.E., Narkhede, A., Tosto, G., Benzinger, T.L., Marcus, D. S., Fagan, A.M., Goate, A., Fox, N.C., Cairns, N.J., Holtzman, D.M., Buckles, V., Ghetti, B., McDade, E., Martins, R.N., Saykin, A.J., Masters, C.L., Ringman, J.M., Ryan, N.S., Forster, S., Laske, C., Schofield, P.R., Sperling, R.A., Salloway, S., Correia, S., Jack Jr., C., Weiner, M., Bateman, R.J., Morris, J.C., Mayeux, R., Brickman, A.M., Alzheimer, D.I., N.,, 2016. White matter hyperintensities are a core feature of Alzheimer's disease: evidence from the dominantly inherited Alzheimer network. Ann. Neurol. 79, 929–939.
Lezak, M.D., Howieson, D.B., Loring, D.W., Fischer, J.S., 2004. Neuropsychological Assessment. Oxford University Press, USA.
Logan, J., Fowler, J.S., Volkow, N.D., Wolf, A.P., Dewey, S.L., Schlyer, D.J., MacGregor, R.R., Hitzemann, R., Bendriem, B., Gatley, S.J., Christman, D.R., 1990. Graphical analysis of reversible radioligand binding from time-activity measurements applied to [N-11C-methyl]-(-)-cocaine PET studies in human subjects. J. Cereb. Blood Flow Metab. 10 (5), 740–747.
Low, A., Mak, E., Malpetti, M., Passamonti, L., Nicastro, N., Stefaniak, J.D., Savulich, G., Chouliaras, L., Su, L., Rowe, J.B., Markus, H.S., O'Brien, J.T., 2021. In vivo neuroinflammation and cerebral small vessel disease in mild cognitive impairment and Alzheimer's disease. J. Neurol. Neurosurg. Psychiatry 92 (1), 45–52.
Malpetti, M., Kievit, R.A., Passamonti, L., Jones, P.S., Tsvetanov, K.A., Rittman, T., Mak, E., Nicastro, N., Bevan-Jones, W.R., Su, L., Hong, Y.T., Fryer, T.D., Aigbirhio, F. I., O'Brien, J.T., Rowe, J.B., 2020. Microglial activation and tau burden predict cognitive decline in Alzheimer's disease. Brain 143 (5), 1588–1602.
Metti, A.L., Yaffe, K., Boudreau, R.M., Simonsick, E.M., Carnahan, R.M., Satterfield, S., Harris, T.B., Ayonayon, H.N., Rosano, C., Cauley, J.A., Health, A.B.C.S., 2014. Trajectories of inflammatory markers and cognitive decline over 10 years. Neurobiol. Aging 35, 2785–2790.
Mintun, M.A., Larossa, G.N., Sheline, Y.I., Dence, C.S., Lee, S.Y., Mach, R.H., Klunk, W.E., Mathis, C.A., DeKosky, S.T., Morris, J.C., 2006. [11C]PIB in a nondemented population: potential antecedent marker of Alzheimer disease. Neurology 67, 446–452.
Mitaki, S., Nagai, A., Oguro, H., Yamaguchi, S., 2016. C-reactive protein levels are associated with cerebral small vessel-related lesions. Acta Neurol. Scand. 133, 68–74.
Owen, D.R., Gunn, R.N., Rabiner, E.A., Bennacef, I., Fujita, M., Kreisl, W.C., Innis, R.B., Pike, V.W., Reynolds, R., Matthews, P.M., Parker, C.A., 2011. Mixed-affinity binding in humans with 18-kDa translocator protein ligands. J. Nucl. Med. 52, 24–32.
Pascoal, T.A., Benedet, A.L., Ashton, N.J., Kang, M.S., Therriault, J., Chamoun, M., Savard, M., Lussier, F.Z., Tissot, C., Karikari, T.K., Ottoy, J., Mathotaarachchi, S., Stevenson, J., Massarweh, G., Scholl, M., de Leon, M.J., Soucy, J.P., Edison, P., Blennow, K., Zetterberg, H., Gauthier, S., Rosa-Neto, P., 2021. Microglial activation and tau propagate jointly across Braak stages. Nat. Med. 27, 1592–1599.
Ridker, P.M., 2004. High-sensitivity C-reactive protein, inflammation, and cardiovascular risk: from concept to clinical practice to clinical benefit. Am. Heart J. 148, S19–S26.
Rosenberg, G.A., 2017. Extracellular matrix inflammation in vascular cognitive impairment and dementia. Clin. Sci. (Lond) 131, 425–437.
Rosenberg, G.A., Prestopnik, J., Knoefel, J., Adair, J.C., Thompson, J., Raja, R., Caprihan, A., 2019. A multimodal approach to stratification of patients with dementia: selection of mixed dementia patients prior to autopsy. Brain Sci. 9.
Rousset, O.G., Collins, D.L., Rahmim, A., Wong, D.F., 2008. Design and implementation of an automated partial volume correction in PET: application to dopamine receptor quantification in the normal human striatum. J. Nucl. Med. 49, 1097–1106.
Schneider, J.A., Arvanitakis, Z., Bang, W., Bennett, D.A., 2007. Mixed brain pathologies account for most dementia cases in community-dwelling older persons. Neurology 69, 2197–2204.
Streit, W.J., 2005. Microglia and neuroprotection: implications for Alzheimer's disease. Brain Res. Brain Res. Rev. 48, 234–239.
van Veluw, S.J., Arfanakis, K., Schneider, J.A., 2022. Neuropathology of vascular brain health: insights from ex vivo magnetic resonance imaging-histopathology studies in cerebral small vessel disease. Stroke 53, 404–415.
Walker, K.A., Windham, B.G., Power, M.C., Hoogeveen, R.C., Folsom, A.R., Ballantyne, C.M., Knopman, D.S., Selvin, E., Jack Jr., C.R., Gottesman, R.F., 2018. The association of mid-to late-life systemic inflammation with white matter structure in older adults: the atherosclerosis risk in communities study. Neurobiol. Aging 68, 26–33.
Walker, K.A., Gottesman, R.F., Wu, A., Knopman, D.S., Gross, A.L., Mosley, T.H., Selvin, E., Windham, B.G., 2019. Systemic inflammation during midlife and cognitive change over 20 years: the ARIC study. Neurology 92, e1256–e1267.
Walsh, J., Tozer, D.J., Sari, H., Hong, Y.T., Drazyk, A., Williams, G., Shah, N.J., O'Brien, J.T., Aigbirhio, F.I., Rosenberg, G., Fryer, T.D., Markus, H.S., 2021. Microglial activation and blood-brain barrier permeability in cerebral small vessel disease. Brain 144, 1361–1371.
Wang, G., Berry, S., Xiong, C., Hassenstab, J., Quintana, M., McDade, E.M., Delmar, P., Vestrucci, M., Sethuraman, G., Bateman, R.J., 2018. A novel cognitive disease progression model for clinical trials in autosomal-dominant Alzheimer's disease. Stat. Med. 37, 3047–3055.
Wang, Q., Chen, G., Schindler, S.E., Christensen, J., McKay, N.S., Liu, J., Wang, S., Sun, Z., Hassenstab, J., Su, Y., 2022. Baseline microglial activation correlates with brain amyloidosis and longitudinal cognitive decline in Alzheimer disease. Neurol.-Neuroimmunol. Neuroinflammation 9.
Wardlaw, J.M., Smith, E.E., Biessels, G.J., Cordonnier, C., Fazekas, F., Frayne, R., Lindley, R.I., O'Brien, J.T., Barkhof, F., Benavente, O.R., Black, S.E., Brayne, C., Breteler, M., Chabriat, H., Decarli, C., de Leeuw, F.E., Doubal, F., Duering, M., Fox, N.C., Greenberg, S., Hachinski, V., Kilimann, I., Mok, V., Oostenbrugge, R., Pantoni, L., Speck, O., Stephan, B.C., Teipel, S., Viswanathan, A., Werring, D., Chen, C., Smith, C., van Buchem, M., Norrving, B., Gorelick, P.B., Dichgans, M., nEuroimaging, S.T.f.R.V.c.o., 2013. Neuroimaging standards for research into small vessel disease and its contribution to ageing and neurodegeneration. Lancet Neurol. 12, 822–838.
Werry, E.L., Bright, F.M., Piguet, O., Ittner, L.M., Halliday, G.M., Hodges, J.R., Kiernan, M.C., Loy, C.T., Kril, J.J., Kassiou, M., 2019. Recent developments in TSPO PET imaging as a biomarker of neuroinflammation in neurodegenerative disorders. Int. J. Mol. Sci. 20.
Weuve, J., Ridker, P.M., Cook, N.R., Buring, J.E., Grodstein, F., 2006. High-sensitivity C-reactive protein and cognitive function in older women. Epidemiology 17, 183–189.
Wu, C., Li, F., Niu, G., Chen, X., 2013. PET imaging of inflammation biomarkers. Theranostics 3, 448–466.
Yokokura, M., Mori, N., Yagi, S., Yoshikawa, E., Kikuchi, M., Yoshihara, Y., Wakuda, T., Sugihara, G., Takebayashi, K., Suda, S., Iwata, Y., Ueki, T., Tsuchiya, K.J., Suzuki, K., Nakamura, K., Ouchi, Y., 2011. In vivo changes in microglial activation and amyloid deposits in brain regions with hypometabolism in Alzheimer's disease. Eur. J. Nucl. Med. Mol. Imaging 38, 343–351.